J Mater Sci: Mater Electron (2015) 26:1142–1150
DOI 10.1007/s10854-014-2518-6

Fabrication and structural characterization of bismuth niobate thin films grown by chemical solution deposition

L. F. Goncalves · J. A. Cortés · M. G. A. Ranieri · F. B. Destro · M. A. Ramirez · A. Z. Simões

Received: 17 September 2014 / Accepted: 15 November 2014 / Published online: 11 December 2014

Abstract Bi_3NbO_7 (BNO) thin films were deposited on $Pt/TiO_2/SiO_2/Si$ (100) substrates at room temperature from the polymeric precursor method. X-ray powder diffraction and transmission electron microscopy were used to investigate the formation characteristics and stability range of the tetragonal modification of a fluorite-type solid solution. The results showed that this tetragonal, commensurately modulated phase forms through the intermediate formation of the incommensurately modulated cubic fluorite phase followed by the incommensurate-commensurate transformation. The 200 nm thick BNO films exhibit crystalline structure, a dielectric constant of 170, capacitance density of 200 nF/cm^2, dielectric loss of 0.4 % at 1 MHz, and a leakage current density of approximately 1×10^{-7} A/cm^2 at 5 V. They show breakdown strength of about 0.25 MV/cm. The leakage mechanism of BNO film in high field conduction is well explained by the Schottky and Poole–Frenkel emission models. The 200 nm thick BNO film is suitable for embedded decoupling capacitor applications directly on a printed circuit board.

1 Introduction

As microsystems move towards higher speed and miniaturization, the requirement of electronic components and devices grows consistently. They should be fabricated in smaller size with maintaining and/or even improving the overall performance. The miniaturization especially becomes even more important today since more and more devices are required to be made portable. Interest of compact packages with high reliability and low cost has been accordingly increased. Many attempts have been made to approach this goal by embedding the passive components into printed circuit boards [1] (PCBs) or low temperature co-fired ceramics [2] (LTCC), since in a typical electrical circuit, 80 % of electronic components are passives (capacitors, resistors, and inductors), which take up to 50 % of printed wiring board area. In addition to the size reduction, the signal path can be considerably shortened by embedding passives and consequently, parasitic noises can be minimized which leads to the improvement of overall performance especially in high frequency devices. Among the embedded passive components, capacitors are most widely studied because they are the major components in terms of size and number and hard to embed compared with resistors and inductors due to the more complicated structure.

The utilization of embedded decoupling capacitors (EDCs) can be a powerful solution for minimizing equivalent series inductance (ESL) of power delivery circuits or packages. To fabricate a capacitor-embedded printed circuit board (PCB) for in-line processing, it is essential to obtain dielectric materials with high permittivity and a low dielectric loss when they are processed at low cost and inexpensive precursors. To achieve these characteristics, studies on bismuth-based dielectrics with a high dielectric constant and a small dielectric loss were made by many research groups [3–12]. BNO has a cubic fluorite structure in nature and is known to have high dielectric constants (100) with low dielectric loss tangent (10×10^{-4}) at an applied frequency of 1 MHz [13]. At room temperature,

L. F. Goncalves · J. A. Cortés · M. G. A. Ranieri · F. B. Destro · M. A. Ramirez · A. Z. Simões (✉)
Faculdade de Engenharia de Guaratinguetá, Univ. Estadual Paulista- Unesp, Av. Dr Ariberto Pereira da Cunha 333, Portal das Colinas, P.O. Box 355, Guaratinguetá, São Paulo 12516-410, Brazil
e-mail: alezipo@yahoo.com

bismuth niobate Bi_3NbO_7 can exhibit two crystallographically modulated modifications, which are both derived from the high-temperature "delta" form of bismuth oxide, δ-Bi_2O_3. Indeed, for temperatures between 1,003 and 1,098 K, δ- Bi_2O_3 belongs to an oxygen deficient fluorite structure (25 % of unoccupied oxygen sites), being one of the best solid-state ionic conductors known so far. In fact, the cubic incommensurate (also called type-II) structure and the tetragonal-commensurate (type-III structure) are interesting because of their high ionic conductivities, with the interest being in solid oxide fuel cells. The tetragonal commensurate form exhibits encouraging dielectric properties, which are combined with good sinterabilty, and as a result, it is a candidate for being a high-permittivity glass free layer in the developing low-temperature cofired ceramic technology for microwave (MW) devices. In addition, type II and III can be converted to each other by appropriate thermal treatments, with which the tuning of dielectric properties can also be achieved. The Bi_3NbO_7 cubic type-II form is a metastable phase below about 1,053 K. Indeed, in the temperature interval from 1,053 to 1,173 K, an order–disorder-like transition occurs to the less symmetrical (and relatively ordered, in terms of the O vacancies) tetragonal type-III phase. The rate of the transformation is very dependent on the temperature, so that below 1,053 K, the waiting time for the transition diverges (the O motions being limited by slow kinetics). On the other hand, the cubic phase is the stable phase above 1,173 K because ordering is prevented by the high oxygen conduction. Therefore, a tetragonal-to-cubic phase transition can also be induced in this material. The structures of the phases II and III of Bi_3NbO_7 have been a matter of debate for many years. However, it is now well accepted that phase II has a cation-averaged fluorite base cell, belonging to the *Fm*3*m* space group (225), which is incommensurately modulated in the three spatial directions (three-dimensional modulation, with a modulation parameter δ close to 0.37). Concerning the tetragonal phase, it is commensurately modulated in a supercell that contains $3 \times 3 \times 7$ fluorite subcells (or a combination of fluorite and pyrochlore cells). The proposed space group for phase III is *I*4*m*2 (119). It is worth pointing out that in this framework, the chemical formula for the tetragonal supercell would be $Bi_{94}Nb_{32}O_{221}$, which is a slightly Nb-rich composition with only one O vacancy per unit cell (in fact, there would be 222 positions for O ions in the proposed unitcell) [14].

In this work, Bi_3NbO_7 (BNO) thin films were prepared by the polymeric precursor method as a new candidate for dielectric capacitors processed at PCB-compatible temperatures. This demonstration of low-cost process, high-performance, and thin-film capacitors is surely an important step toward the development of embedded decoupling capacitor.

2 Experimental procedure

Bismuth niobate thin films were prepared by the polymeric precursor method, as described elsewhere [15]. The films were spin coated on Pt/Ti/SiO_2/Si substrates by a commercial spinner operating at 5,000 revolutions/min for 30 s (spin coater KW-4B, Chemat Technology). An excess of 5 % wt of Bi was added to the solution aiming to minimize the bismuth loss during the thermal treatment. Each annealing cycle of the thin film was performed at 700, 800 and to 860 °C for 2 h in the conventional furnace under static air atmosphere. The film thickness was reached by repeating 10 times the spin-coating and heating treatment cycles. The thickness of the annealed films was measured using scanning electron microscopy (Topcom SM-300) at the transversal section. We have obtained films with thickness of 200 nm. In this case back scattering electrons were used. Thermal effect was investigated by thermogravimetric analysis (TGA) and differential thermal analysis (DTA) in the apparatus STA 409, Netzsch, Germany. The 4 h thermal treatment of the resin at 300 °C resulted in a soft black powder, portions of which were heat-treated from room temperature to 900 °C using a heating rate of 5 °C/min with synthetic air flow (30 cm^3/min). Phase analysis of the films was performed at room temperature by X-ray diffraction (XRD) using a Bragg–Brentano diffractometer (Rigaku 2000) and CuKα radiation in the 2θ range from 20 to 70° with $0.03°/min^{-1}$. The morphology of the films was observed using a high resolution field-emission gun scanning electron microscopy FEG-SEM (Supra 35-VP, Carl Zeiss, Germany). Top Au electrodes (0.5 mm diameter) were prepared for the electrical measurements by evaporation through a shadow mask at room temperature. The XPS analysis was carried out at a pressure of less than 10^{-7} Pa using a commercial spectrometer (UNI-SPECS UHV) to verify the changes in surface chemical composition of the treated specimens. The Mg K line was used (h = 1,253.6 eV) and the analyzer pass energy was set to 10 eV. The inelastic background of the Bi 4f, Nb3d and O 1s electron core-level spectra were subtracted using Shirley's method. The composition of the near surface region was determined with an accuracy of ±10 % from the ratio of the relative peak areas corrected by Scofield's sensitivity factors of the corresponding elements. The spectra were fitted without placing constraints using multiple Voigt profiles. The width at half maximum (FWHM) varied between 1.2 and 2.1 eV and the accuracy of the peak position was ±0.1 eV. To obtain better insight into the nature of the deposited phases and their crystallographic relationship, cross-sectional samples were further investigated by transmission electron microscopy (TEM) and selected area diffraction (SAD) patterns onto 300 mesh Cu grids. Measurements were then taken at an accelerating

voltage of 200 kV on a Philips model CM 200 instrument. The dielectric properties were investigated by using a precision impedance analyzer (4294A, Agilent). The current–voltage (I–V) characteristics were examined with a semiconductor characterization system (4200-SCS, Keithley).

3 Results and discussion

In order to determine the best condition of annealing and to obtain crack free films, a thermal analyses was performed. Figure 1 shows the TG–DTA curves of the BNO polymeric solution obtained from room temperature up to 900 °C. The existence of three stages of weight loss can be observed in Fig. 1a. The first stage (170–275 °C) is related to elimination of water produced during the process of esterification and the excess of ethylene glycol. The second one (275–400 °C) corresponds to a break away of the polymeric chains formed by a polyesterification reaction. The last weight loss between 450 and 550 °C is due to the decomposition of organic compounds. After that, no weight loss can be detected because the decomposition of organic material has finished. The endothermic signals, in the range of 110–150 °C and 190–230 °C, were attributed to the evaporation of water and solvents, respectively (DTA curve, Fig. 1b). A very intense exothermic signal observed in the range of 450–550 °C was assigned to the pyrolysis of organic ligands and crystallization of main phase. Above 560 °C the Bi_3NbO_7 stable phase was formed.

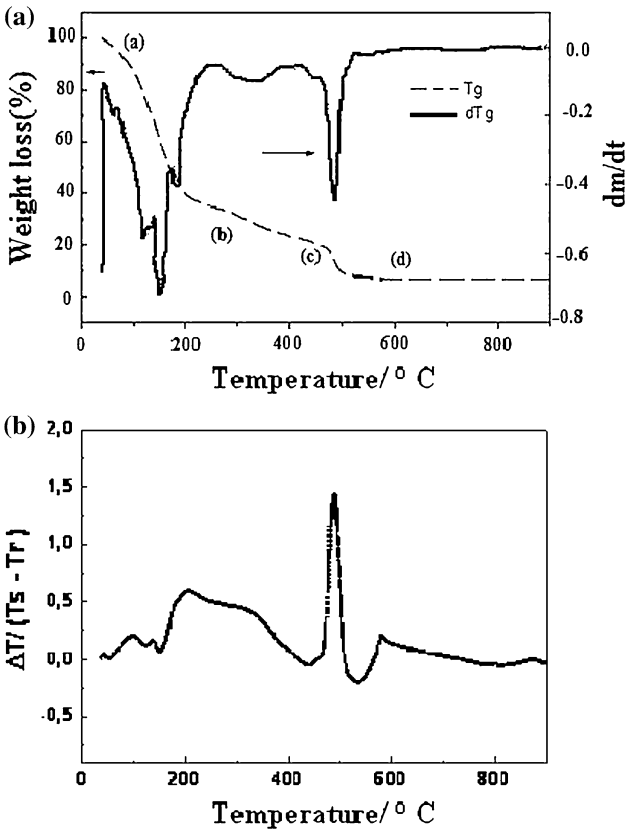

Fig. 1 Thermogravimetric analyses of the BNO precursor solution annealed from room temperature to 900 °C: **a** TG and **b** DTA curves

Figure 2 presents the XRD patterns of BNO films deposited on platinum coated silicon substrates. The films were well crystallized at a processing temperature under investigation. As can be seen, a fluorite-type structure is obtained. No traces of $Bi_5Nb_3O_{15}$ [16] and δ Bi_2O_3 phase (a 55.648 Å, [17]), appears to be present. The Bi_3NbO_7 phase belongs to the classical fluorite-type structure. The BNO film self-organized to produce (111)-preferred orientation with good crystallinity. The additional, i.e., satellite, reflection of low intensity related to (2 0 0), (2 2 0), (3 1 1) planes in Fig. 2 indicate a superstructure. The satellite reflections are present at the same positions as those reported in the literature, which confirms the similar incommensurate modulation of Type II, as described by Miida et al. [18]. The most intense diffraction peaks appear at the same 2θ angles, but due the temperature employed to crystallize the film at 860 °C a very noticeable tetragonal splitting is observed. The XRD patterns can be identified and indexed using the standard XRD data of Bi_3NbO_7 (JCPDS 86-0875), with space group Fm3 m. The six peaks in the patterns were indexed to (311) (1 1 1), (2 0 0), (400), (2 2 0), (2 2 2) and (440) planes respectively, and can match well with the standard peaks of Bi_3NbO_7.

To confirm the surface morphology, FEG-SEM was carried out. The results are shown in Fig. 3. The BNO films consist of a homogeneous surface although some degree of porosity is evident. The average grain size measured is 43 nm. BNO film exhibit a homogenous structure being the deposition of the thin films performed by a nucleation and growth process at the surface of the substrates. Because the

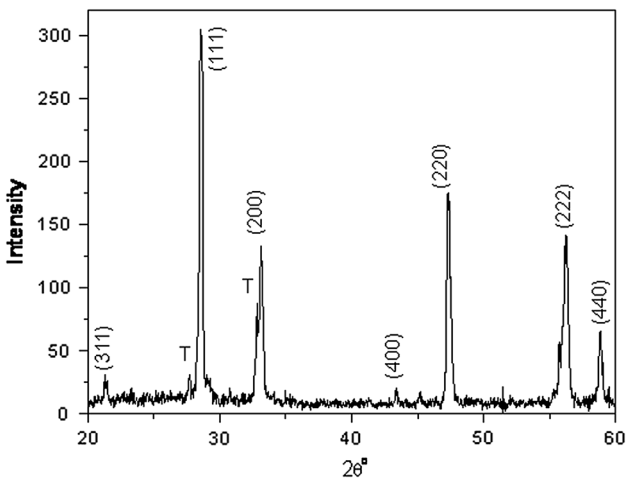

Fig. 2 X-ray diffraction of BNO thin film deposited by the polymeric precursor method and annealed from 700 to 860 °C in static air for 2 h

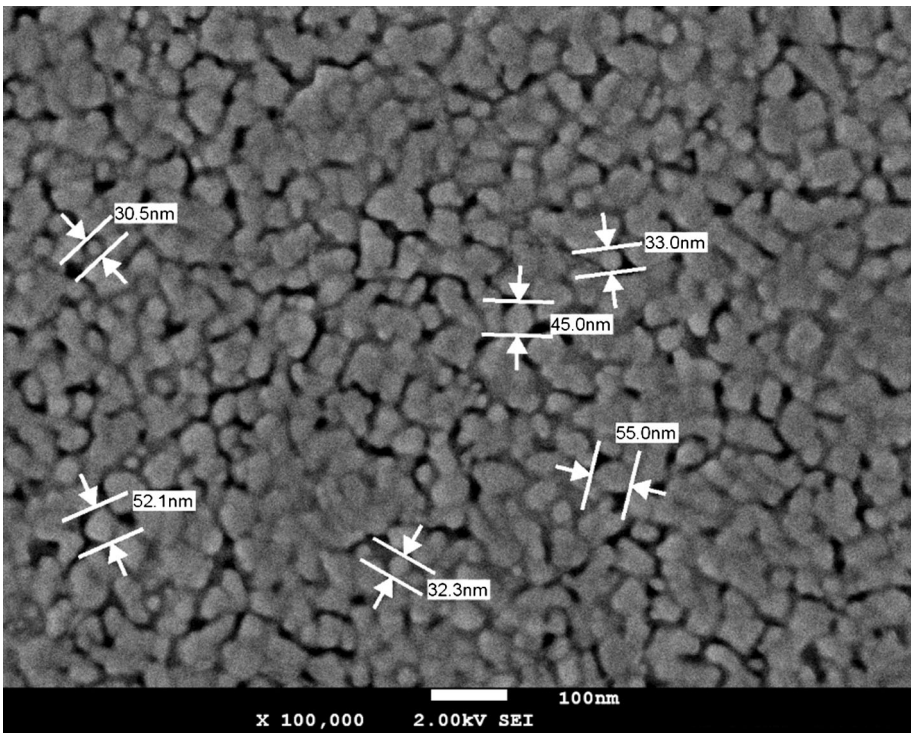

Fig. 3 FEG-SEM micrograph of BNO thin film deposited by the polymeric precursor method and annealed from 700 to 860 °C in static air for 2 h

annealing conditions employed, the diffusion of species and the nucleation and growth rate increased affecting the grain size and shape of grains. Bismuth-based dielectric materials contain a bismuth metal in the as-deposited films also may play an important role in the formation of smooth and dense morphologies.

TEM analyses of the BNO film is shown in Fig. 4. Polycrystallinity of the grains in the plane of the films is observed. The grains are regularly shaped and the estimates size obtained from dark field images is about 50 nm, consistent with FEG-SEM analyses. Tiny pores less than 10 nm in size are present within the grains and along the grain boundaries. From TEM analyses we could observe the presence of crystalline phase. Besides that, the diffraction patterns indicate strong randomness of atom position, as previous noted in the XRD data. In order to understand the possible coordination of both niobium and bismuth atoms in Bi_3NbO_7, we propose different models of possible rearrangement of the oxygen–fluorite-type network. From the classical organization of M_4O_8-type fluorite, the displacement of some oxygen atoms, as shown in Fig. 4b, keeps the overall M_4O_8 composition but changes some metallic coordination from CN = 8 to CN = 7 and CN = 6. Pursuing this line, some oxygen can be removed (oxygen loss), creating vacancies and leading to a non-stoichiometric fluorite-type network, i.e., M_4O_7 composition. Such hypothesis implies local anionic reorganization in the 3-dimensional network in order to give a classical oxygen octahedron around the niobium atoms, with bismuth atoms accepting a wide variety of oxygen polyhedra more or less distorted by the stereochemical influence of its lone pair. Such an arrangement can occur in all directions, giving rise to local differences of composition and order in the crystal. Electron diffraction patterns along [001], [110], [111] zone axes are shown in TEM (Fig. 4b–d). Small differences in the intensities of the superlattice maxima with respect to intensities already published [19] can be appreciated, but this could be due to the incommensurability of the structure and to the different compositions. The observed lattice fringe spacing of 0.31 nm corresponds to the (1 1 1) plane of the Bi_3NbO_7 crystal. This result is consistent with that of XRD patterns in Fig. 2, where the (1 1 1) peak is the strongest as compared to other patterns. The experiments showed that the tetragonal phase with the $3 \times 3 \times 7$ superstructure appears at the temperature employed. Firing at 860 °C for 2 h, for instance, yields a sample in which both cubic and tetragonal phases were detected. From experiments performed to determine the thermal stability of the tetragonal Bi_3NbO_7 we noticed that during the film growth the cubic phase is formed first, and then if the right annealing conditions are used it transforms into the tetragonal phase. A periodicity in the tetragonal phase that is a rational multiple of the unit cell of the underlying fluorite structure indicates that the tetragonal phase in contrast to the cubic phase, exhibits a commensurate superstructure ordering. This means that the transition from cubic to tetragonal phase in the case of Bi_3NbO_7 is a certain kind of disorder–order or

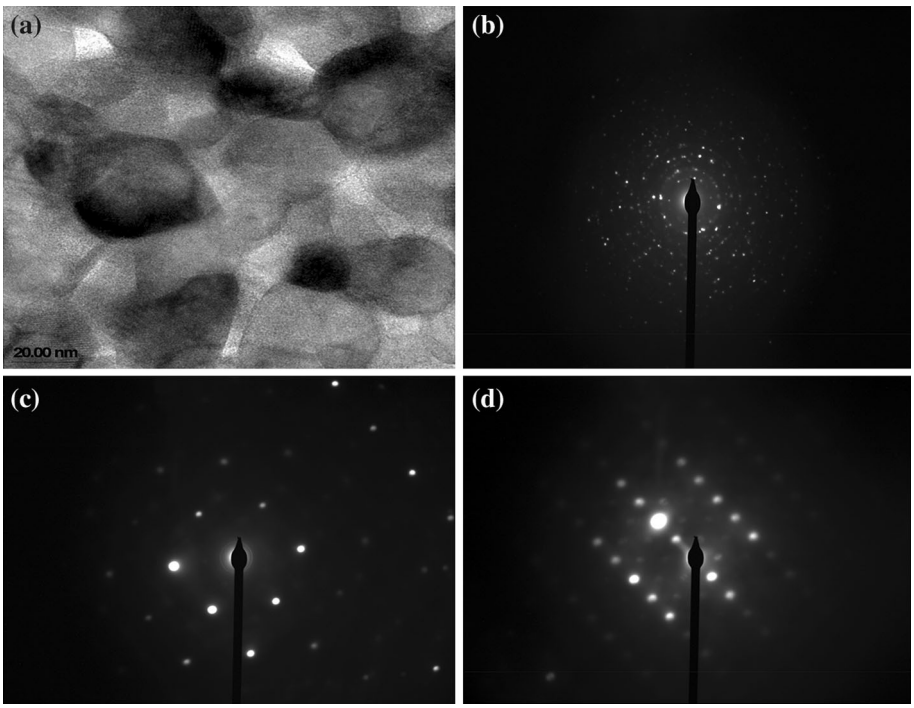

Fig. 4 **a** TEM microscopy of BNO thin film deposited by the polymeric precursor method and annealed from 700 to 860 °C in static air for 2 h. **b** Electron diffraction patterns of Bi_3NbO_7 along the cubic zone axes: **b** [001]; **c** [110]; **d** [111]

incommensurate–commensurate phase transition. Such a phase transition exhibits kinetics that is temperature dependent. Therefore, at higher temperatures, closer to the upper temperature limit (860 °C) of its thermodynamic stability, the formation of the tetragonal (ordered) phase is much more rapid than at the lower temperatures (700 °C).

The valence states of bismuth and niobium on the surface of the Bi_3NbO_7 film were determined by X-ray photoelectron spectroscopy (XPS). High-resolution XPS spectra of Bi4f region is shown in Fig. 5, which could be fitted into two peaks. The binding energy values of ($4_{f7/2}$) 159.5 eV and ($4_{f5/2}$) 164.8 eV with the spin–orbit splitting (5.3 eV) is ascribed to Bi^{3+} [20]. No other peak with lower energy asymmetry is evident which indicates the absence of a lower Bi oxidation state Bi^{2+} [21]. The high-resolution XPS spectrum of the Nb3d region is shown in Fig. 5b. Two peaks located at 207 and 210 eV are identified, which indicates niobium in the as-prepared Bi_3NbO_7 exists in Nb^{5+} [22]. From these results we can infer that the oxygen vacancies would be easily accommodated in the NbO_5 local substructure. Thus, the increasing of Bi–O bonding causes structural disorder in the NbO_6 octahedron network. The charge transfer between [NbO_5 $V_O^{\bullet}$] clusters and $Bi_{Bi}^{'}$ defects creates positive and negative polarons and the combination of both constitutes a new entity called Jahn–Teller bipolaron that causes additional strain. Calibration of binding energy scale was controlled using the O1's line, which appears in the photoelectron spectra of the as grown samples.

Because Bi_3NbO_7 shows an oxygen-deficient fluorite structure with a disordered long-range vacancy, good oxide ion conduction is expected. For other mixed oxides derived from δ-Bi_2O_3, a conductivity dominated by movement of oxygen vacancies has been reported [23]. The frequency dependency of the permittivity and dielectric losses of the BNO film is shown in Fig. 6a. The permittivity and dielectric losses of thin films decreased appreciably with frequency increasing. Similar dependency of permittivity and dielectric losses on frequency has been reported on Bi-contained pyrochlore ceramics [24]. The BNO thin film demonstrated very low dielectric loss values in the measurement frequency range. The dielectric losses were lower than 0.4 % in this temperature range. The dielectric behavior might be associated with the interfacial leakage conduction loss between grains. It was supposed that high density of interfacial defects in thin films with large porosity would enhance leakage conduction loss at interfaces between grains. The measured properties show that the presence of the observed grain boundary inclusions did not negatively affect the dielectric constant, which is close to that of bulk ceramics. Since Fig. 4 reveals structural identity on the level of the prototype cell and on the level of the superstructure modulation it is evident that the incommensurate-cubic phase undergoes a certain kind of disorder–order phase transition at 860 °C to the commensurate-tetragonal phase. In potential electronic device applications of ferroelectric thin films it is desirable to understand the behavior of the dc-leakage current with the

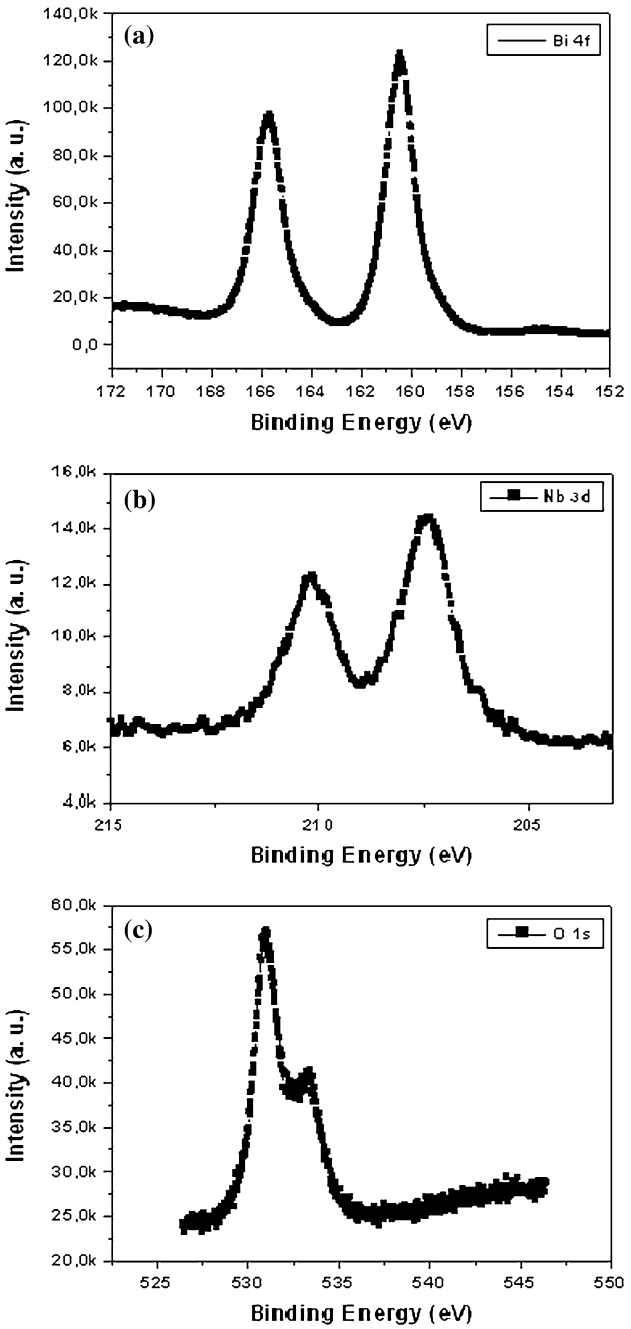

Fig. 5 XPS analysis of BNO thin films annealed from 700 to 860 °C in static air for 2 h: **a** Bi 4f peaks, **b** Nb3d peak and **c** O 1s peak

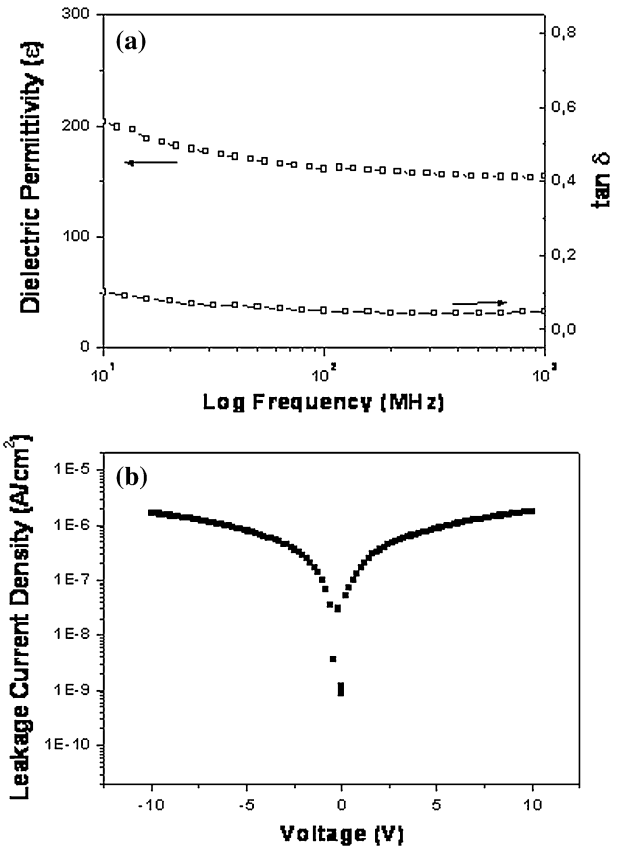

Fig. 6 **a** Dielectric properties in dependence of frequency for BNO thin films annealed from 700 to 860 °C in static air for 2 h and **b** typical *I–V* curve of BNO thin films annealed from 700 to 860 °C in static air for 2 h

bias field. The mechanism of leakage current density in ferroelectric thin films is more difficult to establish in comparison to other physical properties of the material. A large number of researchers have attempted to understand the leakage current characteristics of oxide ferroelectric thin films and low leakage current density is important consideration for memory device applications [25, 26]. A typical leakage current characteristic for BNO thin film is given in Fig. 6b. The curve was recorded with a voltage step width of 0.1 V and elapsed time of 1.0 s for each voltage; here the measured logarithmic current density (log J) versus the voltage (V) is shown. It can be seen that there are two clearly different regions. The current density increases linearly with the external electric field in the region of low electric field strengths, suggesting an ohmic conduction. This ohmic behavior occurs in insulating film as long as the film is quase neutral, that is, as long as the bulk generated current in the film exceeds the current due to injected free carriers from the electrode. This current would be due to the hopping conduction mechanism in a low electric field, because thermal excitation of trapped electrons from one trap site to another dominates the transport in the films. At higher field strengths the current density increases exponentially, which implies that at least one part of the conductivity results from Schottky or Poole–Frenkel emission mechanism. The leakage current density at 5.0 V is equal to 10^{-7} A/cm^2 and a breakdown strength of 0.25 MV/cm. Since different top and bottom electrodes were used we assume that the bulk controls the properties of such film revealing a symmetric *I–V* characteristic for both voltage polarities. Therefore, the low

leakage current can be an effect of the grain size, which implies several grain boundaries along the current flow acting as potential barriers.

In order to analyze the dominant mechanism of the BNO films at higher fields, the J-E properties were plotted using Schottky and Poole–Frenkel (P–F) emission models (Fig. 7a, b, respectively). The former is a Schottky emission (SE) process across the interface between a semiconductor (metal) and an insulating film as a result of barrier lowering due to the applied field and the image force. The latter is associated with the field enhanced thermal excitation of charge carriers from traps, sometimes called the internal Schottky effect. These two transport mechanisms are very similar and can be distinguished from the slope measured from the straight line region of the current–voltage (I–V) curve in the form of $\log_{10}(J)$ or $\log_{10}(J/E)$ versus $E^{1/2}$plots, respectively. Both Schottky (Fig. 7a) and Poole–Frenkel (Fig. 7b) plots for BNO films indicate good linearity by least square fit, suggesting that the leakage current mechanism is either SE or PF type. The difference in dominant mechanism between these films was ascribed to the concentration variation of the oxygen vacancies in the films.

Figure 8a shows the bias-field dependence of the capacitance at a measurement frequency of 1 MHz for BNO film on platinum coated silicon substrates. The curve is symmetric around the zero bias axis, indicating that BNO film contain few movable ions or charge accumulation at the film-electrode interface. The dielectric permittivity calculated from *C–V* curve is around 180 agreeing with the dielectric permittivity as a function of frequency. Although positive and negative biases were employed there is no evidence of hysteresis behavior, confirming the absence of domain structure. The tunability is defined as $(C_0 - C_v)/C_0$ where C_0 and C_v are the capacitance values at zero and maximum DC-voltage levels. For a field of 1 MV/cm and a measurement frequency of 1 MHz, maximum tunability of 28 % was obtained. The tunability

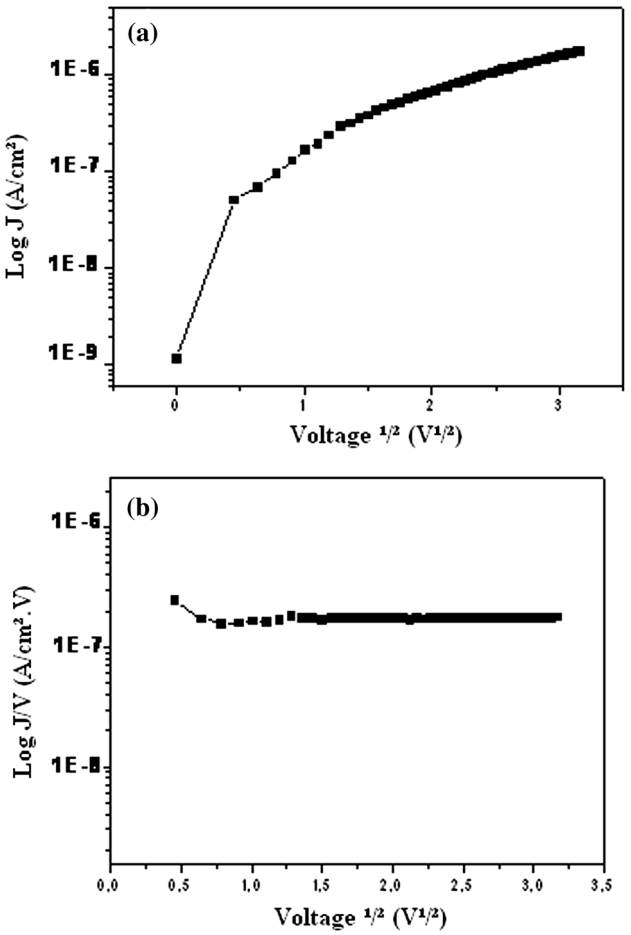

Fig. 7 **a** The Schottky log (J) and **b** Poole–Frenkel (P–F) emission models log (J/V) relationships are plotted as a function of $V^{1/2}$ for BNO thin film deposited by the polymeric precursor method and annealed from 700 to 860 °C in static air for 2 h

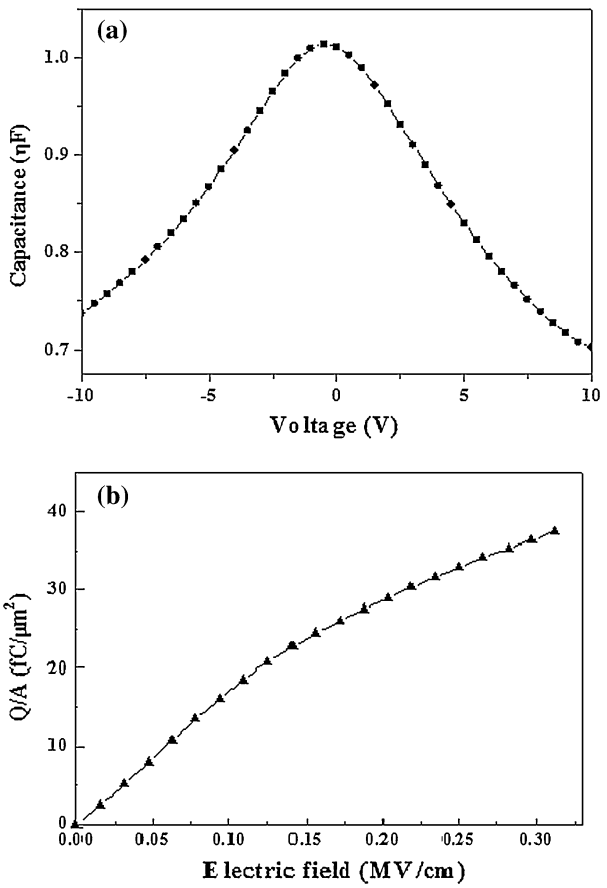

Fig. 8 **a** Capacitance voltage characteristic for BNO thin films annealed from 700 to 860 °C in static air for 2 h and **b** charge storage density for BNO thin films annealed from 700 to 860 °C in static air for 2 h

showed no hysteresis. Studies are underway to clarify the role of film strain due to the differences in thermal mismatch and its dependence on tunability. In view of the XRD and TEM measurements discussed above, it was suggestive that the higher tunability of such film could be a result of a commensurate superstructure ordering, as well as the relatively larger grain size, since the larger grain size could be a positive factor to dielectric tunability. The charge storage density were estimated from the C–V characteristics using the relationship $Q_c = \varepsilon_0\varepsilon_r E$, where ε_0 is the permittivity of free space, ε_r is the relative permittivity and E is the applied field (Fig. 8b). A practical DRAM capacitor requires a leakage current density (LCD) of 3 μA/cm^2 and a charge storage density of about 35 fC/μm^2 [27]. From Fig. 7b it may be seen that this would be satisfied already at E = 0.27 MV/cm.

4 Conclusions

Crystalline BNO film can be prepared by the polymeric precursor method on platinum coated silicon substrates. The study by electron diffraction and high resolution electron microscopy has shown that Bi_3NbO_7 exhibits a defect fluorite-type structure with an incommensurate cubic lattice. XPS analyses reveal charge transfer between [NbO_5 $V_O^{\bullet}$] clusters and $Bi_{Bi}^{'}$ defects creating positive and negative polarons that causes additional strain in the film. The dielectric properties of BNO thin films were strongly affected by the incommensurate–commensurate phase transition and surface grain size. The dielectric loss lower than 0.4 % and the maximum voltage tunability of 28 % with an applied bias field of 0.25 MV/cm under 1 MHz were obtained by the chemical solution deposition. The nonlinear leakage current behaviors observed in the BNO film is explained by either Schottlky or Poole–Frenkel conduction mechanisms. The very low losses and electric field tunable dielectric constant may make these films promising for tunable capacitor applications.

Acknowledgments The financial support of this research project by the Brazilian research funding agencies CNPq and FAPESP is gratefully acknowledged. We also like to thanks José de los Santos Guerra from UFU for dielectric facilities and Marco Cantoni from EPFL from TEM analyses.

References

1. W.J. Borland, S. Ferguson, Embedded passive components in printed wiring boards: a technology review, CircuiTree March (2001)
2. M.R. Gongora-Rubio, P. Espinoza-Vallejos, L. Sola-Laguna, J.J. Santiago-Aviles, Overview of low temperature co-fired ceramics tape technology for meso-system technology (MsST). Sens. Actuators, A **89**, 222–241 (2001)
3. A.A. Maradudin, D.L. Mills, Scattering and absorption of electromagnetic radiation by a semi-infinite medium in the presence of surface roughness. Phys. Rev. B **11**, 1392–1415 (1975)
4. R.L. Moreira, F.M. Matinaga, U. Pirnat, D. Suvorov, A. Dias, Optical phonon characteristics of incommensurate and commensurate modulated phases of Bi_3NbO_7 ceramics. J. Appl. Phys. **103**, 094108-1–095108-7 (2008)
5. S.N. Ng, Y.P. Tan, Y.H. Taufiq-Yap, Mechanochemical synthesis and characterization of bismuth-niobium oxide ion conductors. J. Phys. Sci. **20**, 75–86 (2009)
6. B.H. Park, S.J. Hyun, S.D. Bu, T.W. Noh, J. Lee, H.D. Kim, T.H. Kim, W. Jo, Differences in nature of defects between $SrBi_2Ta_2O_9$ and $Bi_4Ti_3O_{12}$. Appl. Phys. Lett. **74**, 1907–1909 (1999)
7. X.P. Wang, Z.J. Cheng, Q.F. Fang, Phase transition kinetics in Bi_3NbO_7 evaluated by in situ isothermal conductivity measurements. Chin. Phys. Lett. **24**, 1013–1016 (2007)
8. D. Zhou, H. Wang, X. Yao, L. Pang, Sintering behavior and microwave dielectric properties of $Bi_3(Nb_{1-x}Ta_x)O_7$ solid solutions. Mat. Chem. Phys. **110**, 212–215 (2008)
9. D. Zhou, H. Wang, X. Yao, Sintering behavior and dielectric properties of Bi_3NbO_7 ceramics prepared by mixed oxides and high-energy ball-milling method. J. Am. Ceram. Soc. **90**, 327–329 (2007)
10. H.C. Ling, M.F. Yan, W.W. Rhodes, High dielectric constant and small temperature coefficient bismuth based dielectric compositions. J. Mater. Res. **5**, 1752–1762 (1990)
11. H. Kagata, T. Inoue, J. Kato, I. Kameyama, Low-fire bismuth-based dielectric ceramics for microwave use. Jpn. J. Appl. Phys. **31**, 3152–3155 (1992)
12. A. Mergen, W.E. Lee, Crystal chemistry, thermal expansion and dielectric properties of $(Bi_{1.5}Zn_{0.5})(Sb_{1.5}Zn_{0.5})O_7$ pyrochlore. Mater. Res. Bull. **32**, 175–189 (1997)
13. Roberto L. Moreira, Franklin M. Matinaga, Urša Pirnat, Danilo Suvorov, Anderson Dias, Optical phonon characteristics of incommensurate and commensurate modulated phases of Bi_3NbO_7 ceramics. J. Appl. Phys. **103**, 094108–094110 (2008)
14. H. Wang, X. Yao, Structure and dielectric properties of pyrochlore-fluorite biphase ceramics in the Bi_2O_3–ZnO–Nb_2O_5 system. J. Mater. Res. **16**, 83–87 (2001)
15. A.Z. Simões, M.A. Ramirez, C.S. Riccardi, E. Longo, J.A. Varela, Ferroelectric properties and leakage current characteristics of $Bi_{3.25}La_{0.75}Ti_3O_{12}$ thin films prepared by the polymeric precursor method. J. Appl. Phys. **98**, 1141031-1-114103-5 (2005)
16. C.D. Ling, M. Johnson, Modelling, refinement and analysis of the 'Type III' Bi_2O_3-related superstructure in the Bi_2O_3–Nb_2O_5 system. J. Solid State Chem. **17**, 1838–1846 (2004)
17. J.W. Lu, S. Stemmer, Low-loss, tunable bismuth zinc niobate films deposited by rf magnetron sputtering. Appl. Phys. Lett. **83**, 2411–2413 (2003)
18. R. Miida, M. Tanaka, A modulated structure in a fluorite-type fast- ion-conductor & #x03B4;-(Bi_2O_3) $(Nb_2O_5)_x$. Jpn. J. Appl. Phys. **29**, 1132–1138 (1990)
19. A. Gulino, S. La Delfa, I. Fragalà, R.G. Egdell, Low-temperature stabilization of tetragonal zirconia by bismuth. Chem. Mater. **8**, 1287–1291 (1996)
20. M. Valant, B. Jancar, U. Pirnat, D. Suvorov, The order-disorder transition in Bi_2O_3-Nb_2O_5 fluorite-like dielectrics. J. Eur. Cer. Soc. **25**, 2829–2834 (2005)
21. K. Tabata, T. Choso, Y. Nagasawa, The topmost structure of annealed single crystal of $LiNbO_3$. Surf. Sci. **408**, 137–145 (1998)
22. V.V. Atuchin, I.E. Kalabin, V.G. Kesler, N.V. Pervukhina, Nb 3d and O 1 s core levels and chemical bonding in niobates. J. Electron Spectrosc. Relat. Phenom. **142**, 129–134 (2005)
23. J.M. Carlsson, B. Hellsing, H.S. Domingos, Theoretical investigation of the pure and Zn-doped alpha and delta phases of Bi_2O_3. Phys. Rev. B **65**, 205122–205132 (2002)

24. H.W. Lee, W.J. Lee, S.G. Yoon, Dielectric Bi_3NbO_7 thin films deposited on polymer substrates by nanocluster deposition for flexible electronic device applications. Electrochem. Solid-State Lett. **12**, G23–G26 (2009)
25. G. Dietz, M.R. Schumacher, R. Waser, S.K. Streiffer, C. Basceri, A.I. Kingon, Leakage currents in $Ba_{0.7}Sr_{0.3}TiO_3$ thin films for ultrahigh-density dynamic random access memories. J. Appl. Phys. **82**, 2359–2364 (1997)
26. J.F. Scott, Y.K. Fang, Device physics of ferroelectric thin-film memories. Jpn. J. Appl. Phys., Part 1. **38**, 2272–2274 (1999)
27. A.I. Kingon, S. Srinivasan, Lead zirconate titanate thin films directly on dielectric and piezoelectric applications. Nat. Mater. **4**, 233–237 (2005)